Research on Engineering Structures & Materials
www.jresm.org
MIM Research Group

Research Article

Unravelling the nonlinear behavior of stabilized mud bricks through inclusion morphology and mineralogical composition analysis

Ahmed Abdelmadjid Ait Salem [*,1,a], Hachimi Dahhaoui [1,b], Naima Belayachi [2,c], Assia Benchouk [1,d]

[1]EOLE Laboratory, Faculty of Technology, University of Tlemcen, POBox 230, Tlemcen, Algeria
[2]Univ. Orléans, Univ. Tours, INSA-CVL, LaMé – EA794, 8 Rue Léonard de Vinci, 45072 Orléans Cedex 2, France

Article Info

Article History:

Received 29 Oct 2025
Accepted 03 Jan 2026

Keywords:

Compressed earth brick;
Stabilizers;
Homogenization;
Unit cell;
Finite element method

Abstract

Compressed earth bricks remain a cost-effective and widely available construction material, and their stabilized forms are increasingly adopted worldwide. In this article, the nonlinear behavior of stabilized mud bricks is assessed, giving particular emphasis to the effect of inclusion morphology and mineralogical composition. The work combines the geotechnical and mineralogical characterization of the soil and silica fume with a micromechanical analysis based on numerical homogenization. Experimental tests will be compared to numerical predictions with the aim of assessing the material response. The results reveal that the increment of silica fume content from 8% to 10% provides a denser mix (17.97 to 18.18 kN/m^3), with improved compressive performance. Inclusion morphology is also a significant factor in nonlinear behavior, as spherical inclusions provided stiffness predictions that were 12% and 18% closer to experimental curves for the 8% and 10% mixes, respectively. These observations underline the importance of accurate microstructural representation when modeling stabilized earth bricks. This integrated experimental–numerical methodology will provide important insight into the predominant mechanisms in stabilized mud bricks and will contribute to establishing more reliable and economic earthen construction materials.

1. Introduction

Compressed stabilized earth bricks CEBs are gaining popularity worldwide due to their cost-effectiveness and remarkable hygrothermal performance. However, raw earth often requires stabilization to improve its mechanical behavior and durability. Stabilization techniques may include mechanical compaction, particle-size correction, or chemical stabilization through hydraulic binders or mineral additives, each contributing differently to compactness and porosity reduction. Numerous studies have therefore explored various stabilizers to enhance the performance of CEBs. For instance, ceramic wastes (50%) were used to improve compressive strength [1], while esparto fibres were incorporated to reduce thermal conductivity and increase flexural strength [2]. Other chemical stabilizers, including cement- and sand-based mixtures, have also been widely studied [3–6] Other researchers have used natural pozzolan as an environmentally friendly alternative to cement in the manufacture of compressed earth blocks (CEBs) [4], others who have used Ground Granulated Blast Furnace Slag (GGBFS) as a binder [5].

*Corresponding author: ahmedabdelmadjid.aitsalem@univ-tlemcen.dz
[a]orcid.org/0009-0008-1767-6185; [b]orcid.org/0000-0002-6603-1411; [c]orcid.org/0000-0003-4112-3368; [d]orcid.org/0000-0002-9985-3518
DOI: http://dx.doi.org/10.17515/resm2026-1308ma1029rs

Overall, these works show that additives can improve strength and durability; however, the resulting materials remain heterogeneous geomaterials whose macroscopic response is governed not only by stabilizer content but also by microstructural features.

Heterogeneous geomaterials exhibit complex micromechanical interactions between their constituents, whose contrasting behaviors strongly influence macroscopic response. Understanding these mechanisms is challenging because their intrinsic mechanical behavior cannot be directly assessed experimentally at the microscopic scale. Numerical homogenization therefore provides an efficient alternative for studying micro–macro interactions. Multiscale strategies have been successfully applied to a broad range of problems, including creep behavior in clays [8–10], micro–macro deformation in embankments [11], mechanical properties of fibre-reinforced composites [12], and nonlinear computational homogenization frameworks [13–17]. These contributions confirm the relevance of homogenization methods, yet only a limited number of studies have applied them to stabilized earth materials, particularly to quantify how inclusion morphology and mineralogical composition jointly influence nonlinear behavior. Although many studies have examined stabilizers for CEBs, and others have developed homogenization models for heterogeneous geomaterials, there is a lack of integrated experimental–numerical studies that explicitly link silica fume content, inclusion morphology, and mineralogical composition to the nonlinear macroscopic behavior of stabilized earth bricks. In particular, the effect of inclusion shape on the micromechanical response of silica-fume-stabilized mixtures remains insufficiently documented.

The present study addresses this gap by investigating the mechanical behavior of a tuff–silica fume mixture for CEB production through a combined experimental and numerical approach. The experimental program involves geotechnical, microstructural (XRD–TGA), and mechanical characterization of the constituents and their mixtures, which serves as a basis for constructing a representative volume element (RVE). A nonlinear numerical homogenization scheme is then applied to predict the macroscopic behavior, and the numerical results are systematically compared with experimental stress–strain curves to assess the accuracy of the proposed model.

The novelty of this work lies in the combined assessment of silica fume morphology, mineralogical composition, and nonlinear micromechanical modelling within the same framework, enabling a more accurate understanding of the mechanisms controlling stabilized earth behavior. The approach provides quantitative evidence of the influence of inclusion morphology on stiffness and strength, which is rarely addressed in previous CEB studies. The results show that the macroscopic behaviour is strongly influenced by both the volume fraction and morphology of silica fume. The proposed homogenization approach offers a reliable predictive tool that reduces the need for costly and time-consuming experimental campaigns and contributes to improved design strategies for stabilized earth bricks.

2. Materials and method

2.1. Description of Material

2.1.1 Soil

The soil analyzed in this research originates from Beni-Saf, a tiny town situated in the Wilaya of Ain Temouchent, which is approximately 520 km from the capital city of Algiers in northwestern Algeria. Table 1 lists the soil's geotechnical features, revealing that it has a low concentration of large, malleable particles. The soil is slightly organic and contains significant amounts of $CaCO_3$.

2.1.2 Silica Fume

Silica fume powder is a highly prized product for its rich silica content, active micro-silicates, and high specific surface area of 220.000 cm2/g. Its composition is mostly made up of amorphous spherical SiO2 particles, accounting for 93-98% of its total makeup. These minute particles, which are a few fractions of a micron in size, give pozzolan a granulometry of 0.05 to 0.15 µm.

Table 1. Geotechnical soil parameters of soil

Properties	Values	Standards
Gravel (%)	12	NF P 94-041 [18]
Sand (%)	48	
Limon (%)	21	NF P 94-057 [19]
Clay (%)	19	
Liquid limit (%)	37	NF P 94-051 [20]
Plasticity Index (%)	17	
Specific density	2,74	NF P 94-054 [21]
Calcium carbonate content (%)	85	NF P 94-048 [22]
Organic meter content (%)	1,8	NF P 94-047 [23]

2.2. Physico-Chemical Analysis Using The DRX-ATG Technique

To conduct a mineral analysis, the X-ray diffraction (XRD) technique was selected. A Rigaku miniflex 600 diffractometer was employed, with a scan range between 2 to 80°, a pitch of 0.02°, and a speed of 4°/minute. Rigaku's PDXL2 software was utilized to process the gathered data. The SDT Q600 device was utilized to carry out both differential thermal analysis (DTA) and thermogravimetric analysis (TGA) concurrently. The temperature range for the analysis was 20 to 1250°C.

The XRD pattern presented in Fig. 1 reveals that the soil mineralogy is mainly composed of quartz and calcite, accompanied by minor amounts of clay minerals and silicate phases, such as kaolinite. Quartz contributes to the granular skeleton of the material, enhancing stiffness and load-bearing capacity, while calcite may act as a cementing agent, promoting particle bonding and improved compressive strength.

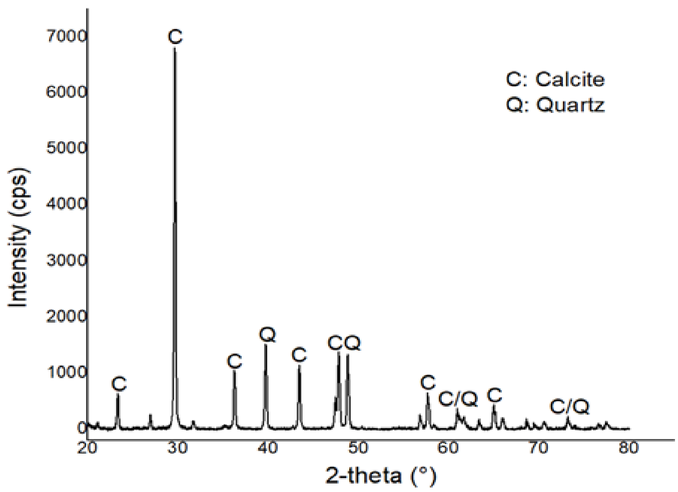

Fig. 1. Soil XRD Spectrum

The TGA/DTA curves shown in Fig. 2 exhibit several characteristic thermal events. The initial mass loss observed below approximately 150 °C is attributed to the evaporation of physically adsorbed water. A subsequent mass loss occurring between 450 and 650 °C is associated with the dehydroxylation of clay minerals, particularly kaolinite. The major mass loss detected at higher temperatures, typically between 700 and 900 °C, corresponds to the thermal decomposition of calcite ($CaCO_3$), confirming its presence as identified by XRD analysis.

The combined XRD and TGA results demonstrate the mineralogical stability of the soil constituents within the temperature range relevant to mechanical testing. The coexistence of a rigid quartz framework, calcite-induced cementation, and limited clay content explains the mechanical performance observed experimentally, particularly in terms of compressive strength and structural integrity. These physico-chemical characteristics justify the use of the identified phases in the subsequent mechanical interpretation and numerical homogenization approach.

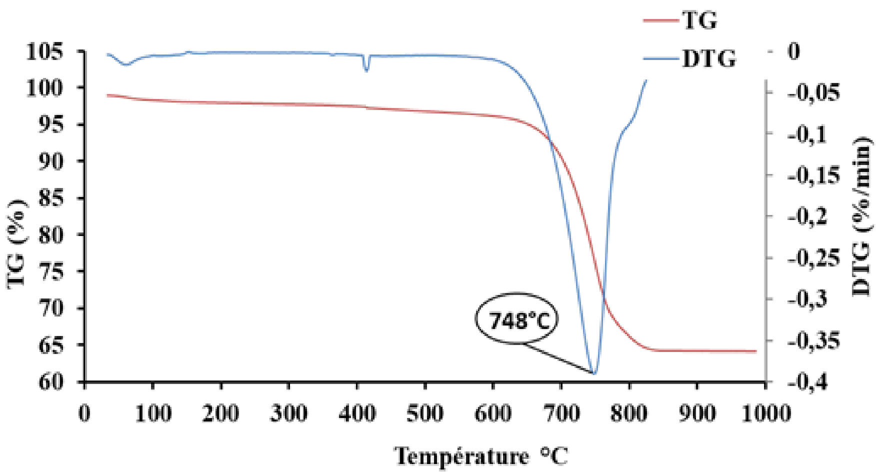

Fig 2. Soil thermogravimetric analysis

2.3. Preparation of Samples

In the industrial sector, compressed earth bricks are typically produced using static compaction. This manufacturing process renders the PROCTOR test unsuitable for determining optimal parameters, as the energy provided differs from that of static compaction. As such, a decision was made to utilize the static compaction method. Initially, a predetermined amount of dry soil was blended with varying amounts of water (ranging from 8% to 18%, with a 2% increment). The mixture was then homogenized and introduced into a double-piston mold for static compaction, ultimately achieving a 4MPa. Finally, density calculations were made for each water content value, based on the weight and volume of the compacted sample. As depicted in Fig 3, the water content fluctuates in relation to the dry density for both mixtures. The graph showcases a bell-shaped curve with a peak dry density that mirrors that of the PROCTOR test. It's important to note that the optimum water content for the mixture of soil and 8% silica fume was 11.42%, resulting in a maximum dry density of 17.97 KN/m3. In contrast, the optimum water content for the mixture of soil and 10% silica fume was 12.3%, yielding a maximum dry density of 18.18 KN/m3. The silica fume contents of 8% and 10% were selected based on the static compaction results presented in Fig. 3, which showed well-defined compaction curves and high maximum dry densities for both mixtures.

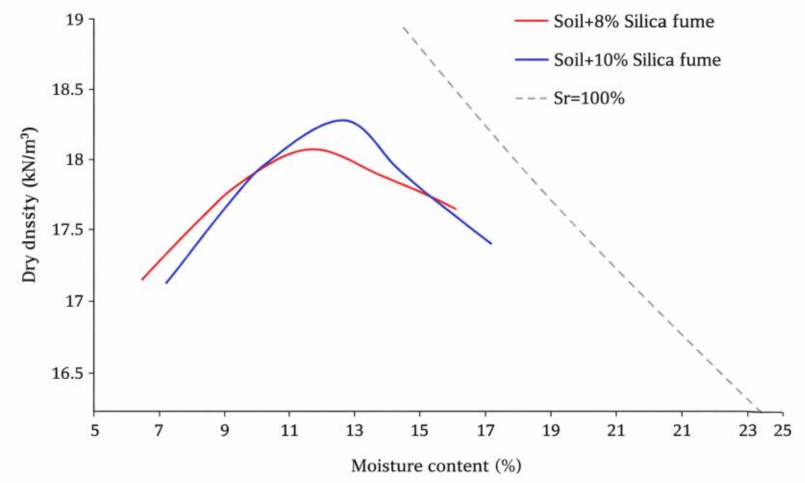

Fig. 3. Static compaction curve

To prepare the samples, the static compaction method was employed with predetermined optimal parameters of dry density and water content. Cylindrical specimens, measuring 10 cm in height and 5 cm in diameter, were manufactured, with a total of five identical samples prepared for each formulation in order to ensure statistical reliability and experimental reproducibility. The specimens were then cured under open-air laboratory conditions for 28 days at a temperature of (20 ±2) °C and a relative humidity of (50 ±2) %. These curing conditions were selected to promote moisture stabilization and to guarantee the reproducibility of the mechanical properties prior to compression testing. After the curing period, uniaxial compression tests were performed.

2.4. Compressive Behavior Method

To conduct a compressive strength test, a hydraulic press equipped with a 50KN force sensor was used in accordance with the Standard EN 1015-11/A1[24]. The test was conducted at a steady speed of 1mm/min. Prior to the test, the sample surfaces were meticulously cleaned to ensure consistent contact with the compression platens.

3. Modelling Procedure

The numerical homogenization framework was employed to predict the macroscopic mechanical behavior of the tuff–silica fume composite based on its microstructural characteristics. The spatial distribution of silica fume particles within the tuff matrix was derived from scanning electron microscopy (SEM) observations (Fig. 4). The porosity of the matrix was explicitly incorporated into the numerical model to ensure consistency with the experimentally compacted material. Three representative volume element (RVE) configurations were investigated to evaluate the influence of inclusion morphology: a spherical inclusion, a cubic inclusion, and a configuration composed of eight randomly distributed spherical inclusions (Fig. 5). The dimensions of the RVE were defined to ensure phase partitioning between the tuff matrix and the silica fume inclusions.

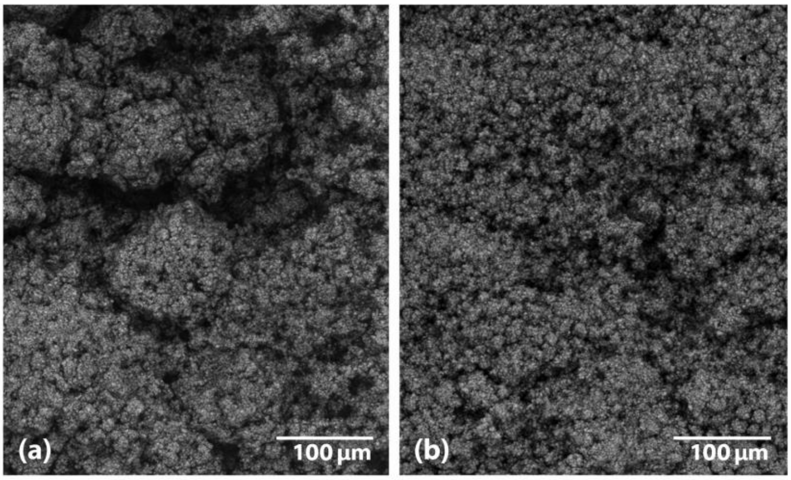

Fig 4. Scanning electron microscopy: (a) Tuff + 8% silica fume, (b) Tuff + 10% silica fume

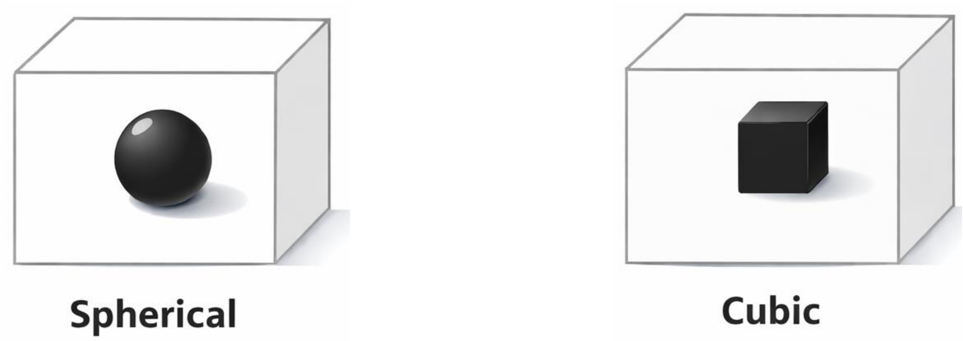

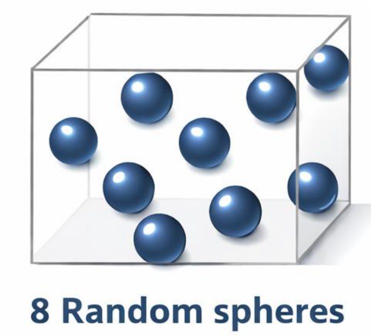

Fig. 5. 3D schematic representation of unit cell for spherical, cubic, and random 8-sphere reinforcement

The mechanical behavior of the tuff matrix was modeled using an elastoplastic formulation with isotropic hardening (NLISO), governed by the Voce law expressed in Eq. (1):

$$H(\varepsilon_e^p) = R_0 \cdot \varepsilon_e^p + R_{inf}.(1 - e^{-b.\varepsilon_e^p}) \tag{1}$$

where σ_0 represents the initial yield stress, R_0 is the initial hardening modulus, R_{inf} denotes the saturation value of isotropic hardening, and b controls the rate of hardening evolution. These parameters characterize the nonlinear compressive response of the tuff matrix and were identified through a least-squares fitting procedure based on experimental uniaxial compression data. The calibrated parameters are summarized in Table 2.

The silica fume phase was assumed to behave as a linear elastic material, consistent with its mineralogical nature and previous studies. Elastic properties for both phases were adopted from the literature [25] and are reported in Table 2.

Table 2. Mechanical parameters of the material

Mechanical properties		Soil matrix	Silica fume
Elastic parameters [25]	E (MPa)	84000	96400
	ν	0,3	0,08
Voce's plastic model parameters	σ0 (MPa)	0.009	
	R0 (MPa)	50.47	
	Rinf (MPa)	1.515	
	b (MPa)	100.05	

Macroscopic stress and strain tensors were obtained through volume averaging of the microscopic fields according to Eq. (2):

$$\bar{\sigma}_{ij} = \frac{1}{V}\int_V \sigma_{ij}\, dV \qquad \bar{\varepsilon}_{ij} = \frac{1}{V}\int_V \varepsilon_{ij}\, dV \tag{2}$$

The RVE geometry was defined such that the volume fractions of the matrix and the reinforcement phases satisfy the unit partition condition given by Eq. (3):

$$f_t + f_s = 1 \tag{3}$$

Numerical simulations were performed using the ANSYS finite element software. Symmetry and periodic boundary conditions were applied following the methodology proposed by Belayachi et al. [15], ensuring a homogeneous macroscopic strain state within the RVE. A uniform displacement was imposed to reproduce uniaxial compression loading conditions consistent with the experimental tests.

The finite element mesh consisted of 10-node tetrahedral elements (SOLID187). A mesh sensitivity analysis was conducted by progressively refining the mesh, particularly around the silica fume inclusions, until variations in the macroscopic stress–strain response became negligible. The adopted mesh (Fig. 6) ensures numerical convergence while maintaining reasonable computational efficiency. The numerical stress–strain responses obtained from the homogenization procedure were quantitatively compared with experimental results, showing good agreement in terms of elastic stiffness, yield stress, and post-yield behavior, thereby validating the proposed numerical model.

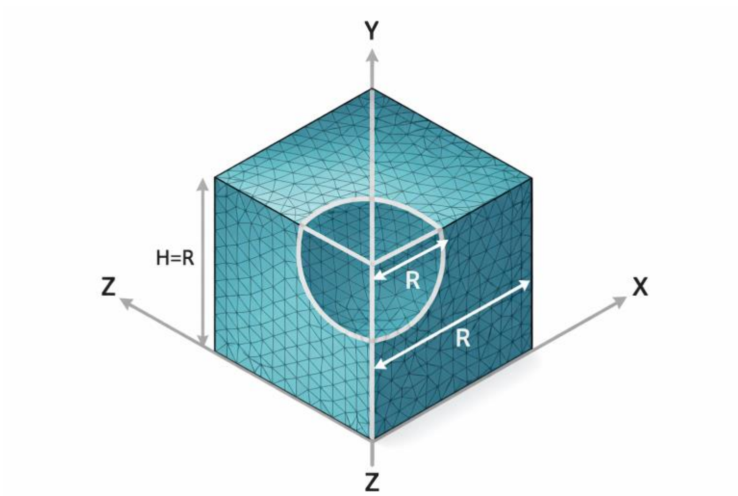

Fig. 6. Example of mesh for the case of a spherical inclusion

4. Results and Discussions

4.1. Compressive Behavior

The stress-strain outcomes are depicted in Fig 7 for the two mixtures that were investigated. It is apparent that the mixture containing soil and 10% silica fume exhibits greater strength than the mixture with soil and 8% silica fume, for the same displacement value. This finding suggests that while silica fume content can improve compressive strength, it is not the sole determinant. In addition, silica fume can bolster soil strength via densification mechanisms. Firstly, silica fume particles fill soil voids, thereby reducing porosity. Secondly, a chemical reaction between silica fume and soil minerals can stabilize the soil, improving its strength and stiffness. This densification was evident in the samples, which were able to endure more stress before breaking.

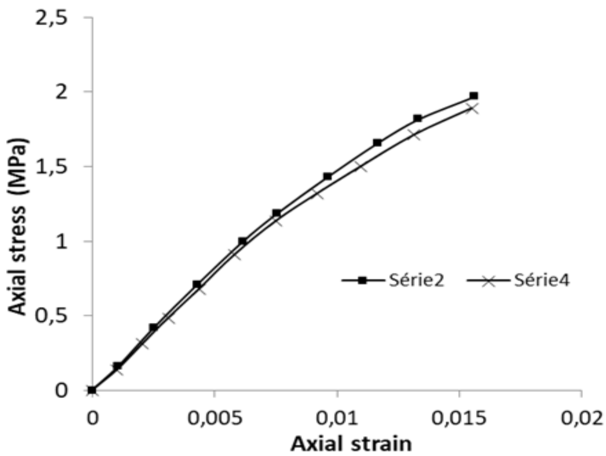

Fig 7. Stress–strain curve of the two mixtures

4.2. Effect of Silica Volume Fraction on Numerical Response

To investigate the impact of silica fume content on the mechanical properties of the material, uniaxial test simulations were performed using various inclusion types, as shown in Table 2. The stress-strain curves of each inclusion type are depicted in Fig 8. The results show a slight difference in the case of a spherical inclusion, but a cubic inclusion's rigidity increased with a 2% silica fume variation. Interestingly, the curves for 8 spherical inclusions had overlapping results for both silica fume contents. These findings emphasize that silica fume content and inclusion type are crucial factors impacting the material's mechanical properties.

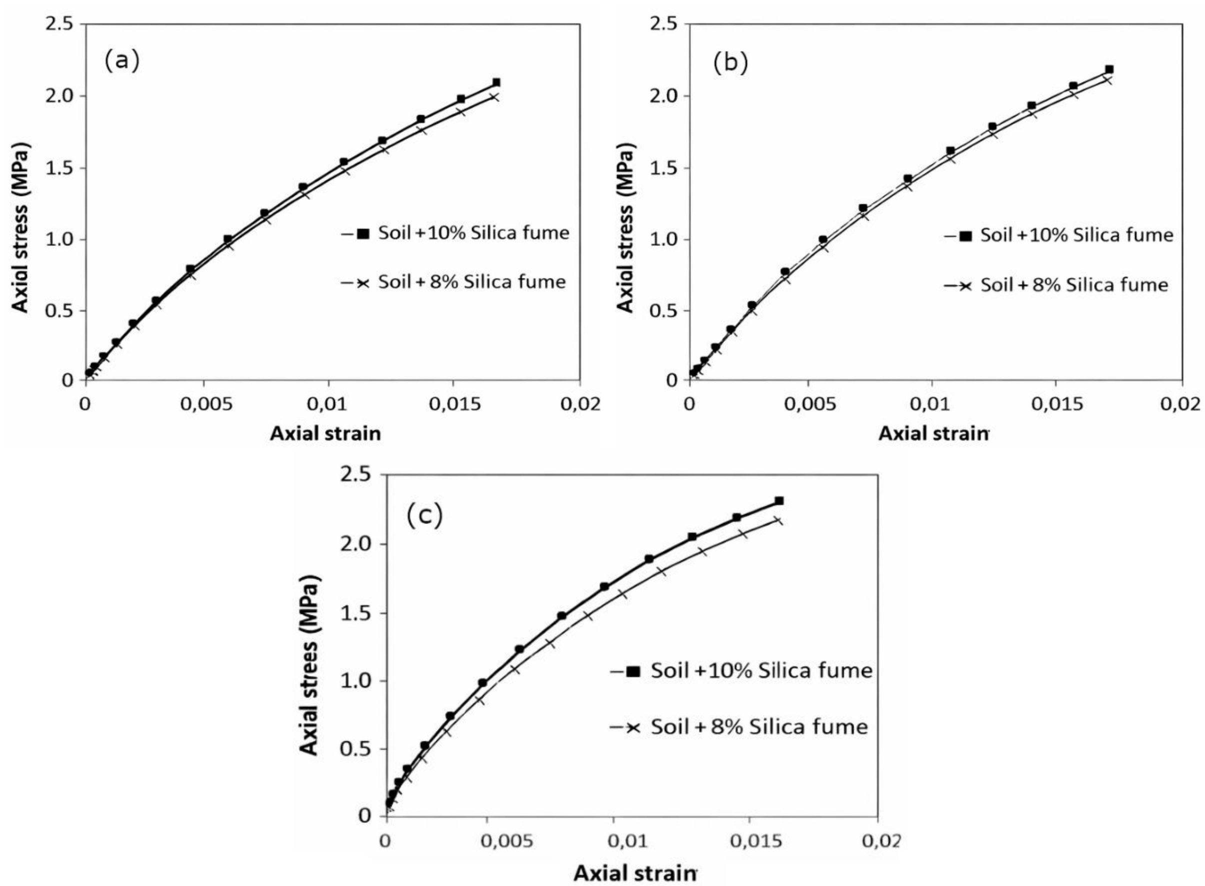

Fig. 8. Macroscopic numerical stress-strain behavior for: (a) One spherical inclusion, (b) Eight spherical inclusions, (c) One cubic inclusion

4.3. Effect of Inclusion Morphology

Fig (9) presents the macroscopic stress-strain curves for different inclusion shapes. The data clearly shows how significant the shape of the silica inclusion can be. For instance, when comparing the spherical inclusion to the cubic inclusion in the mixture of soil+8% silica fume, there was a 12% difference.

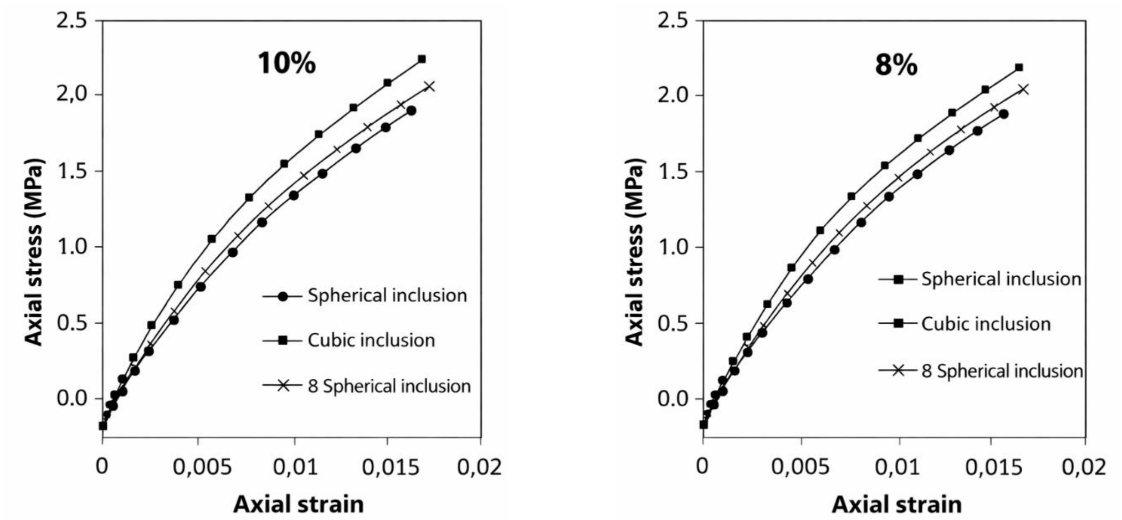

Fig. 9. Effect of inclusion morphology on the stress-strain behavior for the two silica fume contents

This gap was even more pronounced, at 18%, in the case of soil+10% silica fume mixture, particularly at high stress and strain levels. The impact of inclusion shape on the effective response of the material was also more significant. This observation was also supported by the study conducted by Belayachi N. et al. [15]. Recent research has revealed that hard inclusions bear less stress than their softer counterparts. Additionally, shapes with corners tend to create a plastic zone, which in turn generates a strong plasticity gradient, resulting in a reduction of stress at these corners. These findings highlight the significance of considering the shape of inclusions while designing composite materials.

4.4. Comparison of Experimental and Numerical Macroscopic Responses

The stress-strain curves for three different shapes of inclusions, as well as the experimental curves, are displayed in Fig 10. It is noteworthy that the responses for all shapes, and for the two silica fume contents, are almost identical, except for the cubic inclusion. In this case, it was observed that the rigidity increased with the silica fume content. The numerical and experimental stress-strain curves for the spherical inclusion, for the two silica fume contents, overlap, indicating that the spherical inclusion is a better representation of the actual microstructure of silica fume grains. This finding has been echoed in other research studies, including Armengaud Julie's work [26]., which analyzed scanning electron microscopy images of silica smoke particles and found that they were approximately 0.1 μm in spherical shape. These findings are consistent with prior experimental research by Aïtcin and Mindess [27]., as well as Vivek Bindiganaville and Banthia [28].

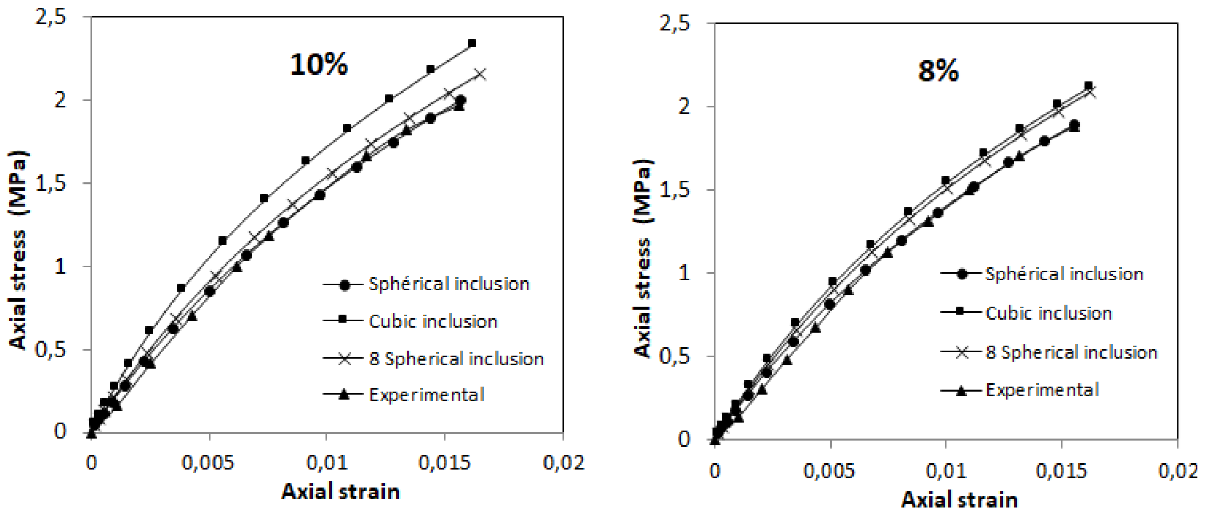

Fig. 10. Comparison of stress/strain behavior for the different inclusions with experimental results

To quantitatively assess the agreement between experimental and numerical responses (Fig. 10), error indicators were computed, including RMSE, MAPE and the coefficient of determination (R^2). For the 8% silica fume mixture, the best matching numerical configuration yields RMSE ≈ 0.12 MPa, MAPE ≈ 9.8% and $R^2 \approx 0.92$, indicating a strong agreement over the investigated strain range. For the 10% mixture, the deviation is higher (RMSE ≈ 0.16 MPa, MAPE ≈ 18.6% and $R^2 \approx 0.86$), suggesting a greater sensitivity of the response to microstructural representation and inclusion morphology. Overall, the quantitative metrics confirm that the proposed homogenization framework captures the global nonlinear trend, with a higher accuracy for the 8% mixture under the present modelling assumptions.

5. Conclusions

This study assessed the nonlinear mechanical behavior of stabilized mud bricks by coupling experimental characterization with micromechanical modelling based on nonlinear numerical homogenization. The experimental program and microstructural observations confirmed that the macroscopic response of the stabilized material depends not only on silica fume content but also on inclusion morphology and mineralogical features, which must be accounted for when interpreting or predicting stress–strain behavior.

The proposed homogenization framework proved capable of reproducing the overall nonlinear trend observed experimentally. Quantitative validation against the experimental curves (Fig. 10) showed good agreement for the 8% mixture (RMSE ≈ 0.12 MPa, MAPE ≈ 9.8%, R^2 ≈ 0.92) and a larger deviation for the 10% mixture (RMSE ≈ 0.16 MPa, MAPE ≈ 18.6%, R^2 ≈ 0.86), indicating an increased sensitivity to microstructural representation at higher stabilizer content. These results provide evidence that inclusion morphology plays a non-negligible role in the predicted macroscopic behavior and support the relevance of microstructure-informed modelling for stabilized earth materials.

The main limitations of the present work are related to the simplified microstructural representation and the modelling assumptions adopted for the phases. Future work will focus on improving microstructural realism (e.g., inclusion size distribution, porosity and phase connectivity), refining phase constitutive behavior, and extending the approach to durability-related performance (wetting–drying cycles, thermal effects and long-term behavior).

Acknowledgement

The authors would like to express their sincere gratitude to the the Algerian Direction of Scientific Research (DGRSDT) for providing financial support to carry out this study.

References

[1] Seco A, Omer J, Marcelino S, Espuelas S, Prieto E. Sustainable unfired bricks manufacturing from construction and demolition wastes. Constr Build Mater. 2018;167:154-165. https://doi.org/10.1016/j.conbuildmat.2018.02.026

[2] Ajouguim S, Talibi S, Djelal-Dantec C, Hajjou H, Waqif M, Stefanidou M, et al. Effect of Alfa fibers on the mechanical and thermal properties of compacted earth bricks. Constr Build Mater. 2020;239:117669. https://doi.org/10.1016/j.matpr.2020.07.539

[3] Islam MS, Tausif-E-Elahi, Shahriar AR, Nahar K, Hossain TR. Strength and durability characteristics of cement-sand stabilized earth blocks. J Mater Civ Eng. 2020;32(5):04020087. https://doi.org/10.1061/(ASCE)MT.1943-5533.0003176

[4] Bennis A, Zniker H, Ghassane A, et al. Eco-friendly production of compressed earth blocks with Moroccan pozzolana as a cement alternative. Res Eng Struct Mater. 2025;11(3):1-19. https://doi.org/10.17515/resm2025-1001ma0702rs

[5] Das S. Mix screening study of laterite soil stabilization using one-part geopolymer binders for earth blocks. Res Eng Struct Mater. 2025. http://dx.doi.org/10.17515/resm2025-1008ma0706rs

[6] Taallah B, Guettala A. The mechanical and physical properties of compressed earth block stabilised with lime and filled with untreated and alkali-treated date palm fibers. Constr Build Mater. 2016;104:52-62. https://doi.org/10.1016/j.conbuildmat.2015.12.007

[7] Norouzi E, Li B, Erkmen RE. Modelling equivalent elastic properties of imperfectly bonded soil-rock mixtures using an XFEM-based computational homogenization. Comput Geotech. 2022;144:104638. https://doi.org/10.1016/j.compgeo.2022.104638

[8] Dahhaoui H, Belayachi N, Zadjaoui A, Duc M. Modélisation du Comportement Différé de la Bentonite Compacte par une Méthode d'Homogénéisation Numérique. Acad J Civ Eng. 2017;35(1):35-38.

[9] Dahhaoui H, Belayachi N, Zadjaoui A, Nishimura T. One-dimensional compression creep change under temperature and suction effects. Int J Geotech Eng. 2022;16(6):670-681. https://doi.org/10.1080/19386362.2021.2025306

[10] Dahhaoui H, Belayachi N, Zadjaoui A. Modeling of Creep Behavior of an Argillaceous Rock by Numerical Homogenization Method. Period Polytech Civil Eng. 2018;62(2):462-469. https://doi.org/10.3311/PPci.11697

[11] Xu WJ, Wang S, Zhang HY, Zhang ZL. Discrete element modelling of a soil-rock mixture used in an embankment dam. Int J Rock Mech Min Sci. 2016;86:141-156. https://doi.org/10.1016/j.ijrmms.2016.04.004

[12] Dehaghani PF, Ardakani SH, Bayesteh H, Mohammadi S. 3D hierarchical multiscale analysis of heterogeneous SMA based materials. Int J Solids Struct. 2017;118-119:24-40. https://doi.org/10.1016/j.ijsolstr.2017.04.025

[13] Yuan Z, Fish J. Toward realization of computational homogenization in practice. Int J Numer Methods Eng. 2008;73(3):361-380. https://doi.org/10.1002/nme.2074

[14] Zhang F, Wang T, Liu F, Peng M, Furtney J, Zhang L. Modeling of fluid-particle interaction by coupling the discrete element method with a dynamic fluid mesh: Implications to suffusion in gap-graded soils. Comput Geotech. 2020;124:103617. https://doi.org/10.1016/j.compgeo.2020.103617
[15] Belayachi N, Do DP, Hoxha D. A note on the numerical homogenisation of the mechanical behaviour of an argillaceous rock. Comput Geotech. 2012;41:70-78. https://doi.org/10.1016/j.compgeo.2011.11.007
[16] Abou-Chakra Guéry A, Cormery F, Shao JF, Kondo D. A micromechanical model of elastoplastic and damage behavior of a cohesive geomaterial. Int J Solids Struct. 2008;45(5):1406-1429. https://doi.org/10.1016/j.ijsolstr.2007.09.025
[17] Ghosh S, Lee K, Moorthy S. Two scale analysis of heterogeneous elastic-plastic materials with asymptotic homogenization and Voronoi cell finite element model. Comput Methods Appl Mech Eng. 1996;132(1-2):63-116. https://doi.org/10.1016/0045-7825(95)00974-4
[18] AFNOR Standards XP P 94-041. Soils investigation and testing. Granulometric description. Wet sieving method. Saint-Denis: AFNOR; 1995.
[19] AFNOR Standards NF P 94-057. Soils investigation and testing. Granulometric analysis. Hydrometer method. Saint-Denis: AFNOR; 1992.
[20] AFNOR Standards NF P 94-051. Soils investigation and testing. Determination of Atterberg's limits. Liquid limit test using Cassagrande apparatus. Plastic limit test on rolled thread. Saint-Denis: AFNOR; 1993.
[21] AFNOR Standards NF P 94-054. Soils investigation and testing. Determination of particle density. Pycnometer method. Saint-Denis: AFNOR; 1991.
[22] AFNOR Standards NF P 94-048. Soils investigation and testing. Determination of the carbonate content - Calcimeter method. Saint-Denis: AFNOR; 1996.
[23] AFNOR Standards NF P 94-047. Soils investigation and testing - Determination of the organic matter content - Ignition method. Saint-Denis: AFNOR; 1998.
[24] AENOR. UNE EN 1015-11/A1: Methods of test for mortar for masonry. Part 11: Determination of flexural and compressive strength of hardened mortar. Madrid: AENOR; 2007.
[25] Giraud A, Hoxha D, Do DP, Magnenet V. Effect of pore shape on effective thermo-poroelastic properties of isotropic rocks. Int J Solids Struct. 2008;45(1):1-23. https://doi.org/10.1016/j.ijsolstr.2007.07.005
[26] Armengaud J. Optimisation des propriétés des bétons projetés par voie sèche [dissertation]. Toulouse: Université Toulouse 3 Paul Sabatier; 2016.
[27] Aïtcin PC, Mindess S. Ecostructures en béton: Comment diminuer l'empreinte carbone des structures en béton. Mayenne: Eyrolles; 2013.
[28] Bindiganavile V, Banthia N. Rebound in Dry-mix Shotcrete: Influence of Type of Mineral Admixture. ACI Mater J. 2000;97(2):115-119. https://doi.org/10.14359/813